DOI: 10.1002/chem.200801418

Speciation of Rare-Earth Metal Complexes in Ionic Liquids: A Multiple-Technique Approach

Peter Nockemann,*[a] Ben Thijs,[a] Kyra Lunstroot,[a] Tatjana N. Parac-Vogt,[a] Christiane Görller-Walrand,[a] Koen Binnemans,[a] Kristof Van Hecke,[a] Luc Van Meervelt,[a] Sergey Nikitenko,[b] John Daniels,[c] Christoph Hennig,[d] and Rik Van Deun*[e]

Abstract: The dissolution process of metal complexes in ionic liquids was investigated by a multiple-technique approach to reveal the solvate species of the metal in solution. The task-specific ionic liquid betainium bis(trifluoromethylsulfonyl)imide ([Hbet][Tf_2N]) is able to dissolve stoichiometric amounts of the oxides of the rare-earth elements. The crystal structures of the compounds $[Eu_2(bet)_8(H_2O)_4][Tf_2N]_6$, $[Eu_2(bet)_8(H_2O)_2][Tf_2N]_6{\cdot}2H_2O$, and $[Y_2(bet)_6(H_2O)_4][Tf_2N]_6$ were found to consist of dimers. These rare-earth complexes are well soluble in the ionic liquids [Hbet][Tf_2N] and [C_4mim][Tf_2N] (C_4mim = 1-butyl-3-methylimidazolium). The speciation of the metal complexes after dissolution in these ionic liquids was investigated by luminescence spectroscopy, ^1H, ^{13}C, and ^{89}Y NMR spectroscopy, and by the synchrotron techniques EXAFS (extended X-ray absorption fine structure) and HEXS (high-energy X-ray scattering). The combination of these complementary analytical techniques reveals that the cationic dimers decompose into monomers after dissolution of the complexes in the ionic liquids. Deeper insight into the solution processes of metal compounds is desirable for applications of ionic liquids in the field of electrochemistry, catalysis, and materials chemistry.

Keywords: EXAFS spectroscopy · HEXS (high-energy X-ray scattering) · ionic liquids · rare earths · UV/Vis spectroscopy

[a] Dr. P. Nockemann, Dr. B. Thijs, Dr. K. Lunstroot, Prof. Dr. T. N. Parac-Vogt, Prof. Dr. C. Görller-Walrand, Prof. Dr. K. Binnemans, Dr. K. Van Hecke, Prof. Dr. L. Van Meervelt
Department of Chemistry, Katholieke Universiteit Leuven
Celestijnenlaan 200F bus 2404, 3001 Leuven (Belgium)
Fax: (+32) 16-327992
E-mail: peter.nockemann@chem.kuleuven.be

[b] S. Nikitenko
Netherlands Organization for Scientific Research (NWO)
DUBBLE@ESRF
6 rue Jules Horowitz, 38043 Grenoble CEDEX (France)

[c] Dr. J. Daniels
High Energy Scattering Beamline ID15
European Synchrotron Radiation Facility
6 rue Jules Horowitz, 38043 Grenoble CEDEX (France)

[d] Dr. C. Hennig
Institute of Radiochemistry, Forschungszentrum Dresden-Rossendorf
P.O. Box 510119, 01314 Dresden (Germany)

[e] Prof. Dr. R. Van Deun
Department of Inorganic and Physical Chemistry, Universiteit Gent
Krijgslaan 281 Building S3, 9000 Gent (Belgium)
Fax: (+32) 9-264-49-83
E-mail: rik.vandeun@ugent.be

Introduction

Ionic liquids have attracted interest from both academic and industrial researchers over the last few years.[1–3] Ionic liquids are organic salts with low melting points which can exhibit intrinsically useful characteristics such as a wide liquidus range (up to 400 °C), a negligible vapor pressure, a large electrochemical window, and high electric conductivity.[4] An important feature of ionic liquids is the tunability of their chemical and physical properties by selection of an appropriate anion/cation combination. Ionic liquids are being applied as solvents for organic reactions,[5–7] liquid–liquid extraction,[8–10] electrodeposition,[11–13] as electrolyte in photovoltaic devices (solar cells),[14,15] and as a component in hybrid materials.[16]

Recent studies demonstrate that also inorganic and materials chemists can take advantage of the properties of ionic liquids.[17–19] For instance, ionic liquids have been applied as solvents and templates to modify the morphology of inorganic nanomaterials.[20–23] Furthermore, the so-called metal-containing ionic liquids are regarded as promising new com-

pounds that combine the properties of ionic liquids with additional intrinsic magnetic, spectroscopic, or catalytic properties, which depend on the incorporated metal ion.[24–30] Additionally, ionic liquids are promising solvents for the crystallization and crystal engineering of metal complexes (coordination polymers) and they are able to trap unique coordination environments.[31–38]

Besides these applications, ionic liquids have been reported to be interesting hosts for photochemical and spectroscopic studies and can be regarded as potential new optical materials.[39,40] For instance, these solvents were found to increase the photochemical stability of tetrakis β-diketonate complexes.[41] Ionic liquids have also been reported to provide low-energy phonon matrices to enable highly efficient near-infrared luminescence of neodymium(III), erbium(III), and ytterbium(III) complexes.[42,43] Although hydrophobic ionic liquids are not miscible with water, they are nevertheless hygroscopic liquids. The presence of water in ionic liquids has to be carefully considered, because even traces of water strongly affect the luminescence properties, as has been shown for some lanthanides, drastically reducing the emission yield.[44] The solvation of f-block element metal ions in ionic liquids has been studied theoretically, for example, by means of molecular dynamics.[8,45,73] Ionic liquids have also been applied as extractants for f-block elements.[46,47]

Recently, we reported on the selective solubilization of various metal oxides and metal salts in the task-specific ionic liquid betainium bis(trifluoromethylsulfonyl)imide, [Hbet][Tf_2N] (abbreviated to betainium bistriflimide).[48] This ionic liquid is able to dissolve rare-earth oxides and uranium(VI) oxide, leading to the formation of betaine bistriflimide metal complexes. The deprotonated betaine is a zwitterionic ligand ($Me_3N^+CH_2COO^-$). Betaine and its derivatives can be regarded as charge-neutral analogues of amino acids.

Although metal compounds dissolved in ionic liquids have found widespread use as catalytic systems and as electrolyte baths for electrodeposition of metals, the knowledge of the speciation of the metals in ionic liquids has been quite limited until now. Recently, a number of reports on the speciation of rare-earth ions in ionic liquids have appeared.[49,50,51,52] The trivalent rare-earth ions are well known for their luminescence properties.[53,54] The shielding of the 4f shell by the closed 5s and 5p shells gives rise to line-like absorption and emission spectra for the electronic f–f transitions. As a result, the luminescence exhibited by these ions has high colorimetric purity, which explains their application in, for example, lighting, imaging, and lasers.[53,55–57] The trivalent europium ion in particular offers the possibility to probe the local symmetry in its first coordination sphere, because of its nondegenerate $^7F_0$ ground state and its nondegenerate $^5D_0$ emitting level, in addition to the good separation of its $^{(2S+1)}L_J$ multiplets. By studying the fine-structure in the luminescence spectrum, one can distinguish between several noncentrosymmetric crystallographic point groups.[58]

EXAFS (extended X-ray absorption fine structure) spectroscopy gives structural information in both ordered and disordered systems through analysis of the X-ray absorption behavior as a function of increasing X-ray energy near an X-ray absorption edge.[59,60,61] When a central atom absorbs an incoming X-ray, a core electron is excited and ejected into the environment. This photoelectron, which can be considered as an outgoing wave, is back-scattered from the neighboring atoms, which can be seen as point scatterers, and the interference between the outgoing electron wave and the back-scattered wave gives rise to an interference pattern, referred to as "fine structure". The analysis of this fine structure provides structural information about the local environment around the absorbing atom (i.e., the number of scattering neighboring atoms, the type of atoms and the distance from the absorbing atom).

Although the need for a continuous X-ray spectrum and thus for synchrotron radiation facilities limits the pace with which EXAFS is becoming a common analysis technique, it has nevertheless already been applied to many scientific questions in the field of f-block element coordination chemistry, in the solid state,[62–66] in solution,[67–72] and in ionic liquids.[70,73–79]

The advantage of EXAFS spectroscopy is that the element of interest can be investigated selectively by exciting an electron from a well-defined core level. EXAFS reflects only the direct coordination of the excited atom, whereas all other compounds in the sample do not contribute to the spectral features of the signal. Unfortunately, the electron scattering amplitude is strongly damped with increasing distance from the excited atom. Therefore, the distance determination in solution is restricted to 3–4 Å. (High-energy) X-ray scattering in solution can reveal distances up to 6–8 Å, which is an enormous advantage when considering the possible presence of polynuclear species. However, all atoms in the sample contribute to the X-ray scattering signal, resulting in complicated scattering signals. This problem can be solved either by selecting an element with high atomic number or in a high concentration, or by estimating the difference between the spectra of the solution with and without the investigated element.[80–83] The application of high energy overcomes absorption effects and allows extension of the momentum transfer Q, which improves the distance resolution.

Herein, we report on the speciation of rare-earth betaine bistriflimide complexes in ionic liquids by combining luminescence spectroscopy, ^1H, ^{13}C, and ^{89}Y NMR spectroscopy, EXAFS, and high-energy X-ray scattering (HEXS). Specifically, we have tried to find an answer to the following questions: 1) what is the local structure of the rare-earth ion's first coordination sphere in the complexes that are formed after dissolution of rare-earth oxides in the ionic liquid [Hbet][Tf_2N] and 2) how does the first coordination sphere change when these complexes are dissolved in the ionic liquids betainium bistriflimide ([Hbet][Tf_2N]) and 1-butyl-3-methylimidazolium bistriflimide ([C_4mim][Tf_2N])?

This experimental and interdisciplinary case study is intended to contribute to a better understanding of the dissolution processes of metal complexes in ionic liquids, which is relevant for the application of these solvents in the fields of electrodeposition, catalysis, and materials chemistry.

Results and Discussion

Synthesis: Protonated betaine bis(trifluoromethylsulfonyl)-imide has the ability to dissolve metal oxides.[48] The rare-earth oxides react with the carboxylic acid group of the ionic liquid to form carboxylate complexes and water. The dissolution of the oxides in the ionic liquid proceeds smoother in the presence of water, most likely because of the increased mobility of the carboxylic proton. The solution was filtered to remove excess rare-earth oxides. After evaporation of water under reduced pressure, a solution of the rare-earth betaine complex in [Hbet][Tf_2N] was obtained. The solubility of the oxides is high, because the ionic liquid can form stoichiometric compounds with the metals. Since the betaine ligand is a zwitterionic ligand, the number of betaine ligands can be higher than the number of anions that are needed for charge compensation.

Crystallography: Without thorough drying, the reaction between Eu_2O_3 and [Hbet][Tf_2N] leads to the crystallization of $[Eu_2(bet)_8(H_2O)_4][Tf_2N]_6$. The crystal structure of this complex, denoted as **1**, consists of $[Eu_2(bet)_8(H_2O)_4]^{6+}$ cations and bistriflimide counterions ($[Tf_2N]^-$). As shown in Figure 1, the two europium(III) ions in the $[Eu_2(bet)_8(H_2O)_4]^{6+}$ cation are linked together by two μ_2-bridging betaine carboxylate groups and two chelating bridging betaine ligands. In this centrosymmetric structure, each europium(III) ion is further surrounded by two monodentate coordinating betaine ligands and two water molecules. Although the europium(III) ions in each dimer are equivalent, there are two crystallographically independent europium(III) dimers present in the asymmetric unit. Nevertheless, the local surroundings of the europium(III) ions in these independent dimers are virtually identical.

The coordination polyhedra of all the europium(III) ions in this structure can be described as a distorted three-capped trigonal prism. In all cases, the coordination number is nine. The Eu–O (carboxylate) bond lengths range from 2.359(5) to 2.593(5) Å. The Eu–O (aqua) bond lengths range from 2.397(5) to 2.501(5) Å. The Eu···Eu distances of the dimeric cations are 4.108(1) and 4.125(1) Å. There are hydrogen bonds between the coordinating water molecules and the monodentate coordinating betaine ligands of neighboring $[Eu_2(bet)_8(H_2O)_4]^{6+}$ cations within O···O distances of 2.687(8) and 2.733(7) Å. Further hydrogen bonding is found from one aqua ligand to a bistriflimide anion with O···O distances of 2.862(8) and 2.893(10) Å for the two dimers. The interlinkage of the dimers by hydrogen bonding is shown in Figure 3 (top).

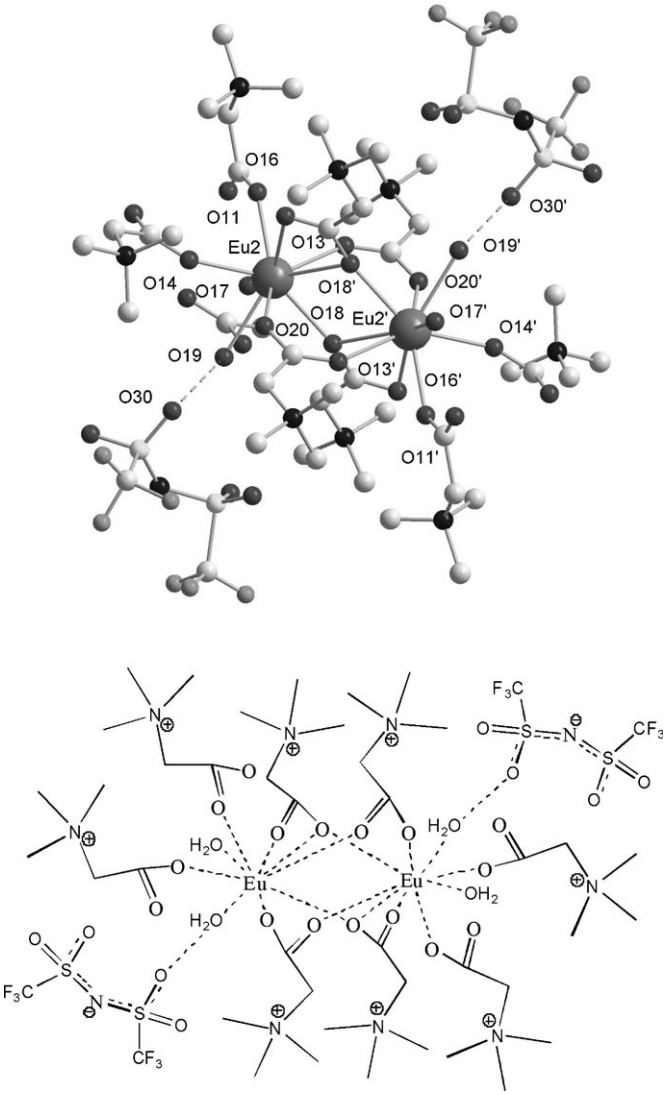

Figure 1. Top: Crystal structure of one europium(III) dimer of $[Eu_2(bet)_8(H_2O)_4][Tf_2N]_6$ (**1**); hydrogen atoms are omitted for clarity (upper part). Bottom: Schematic representation of the $[Eu_2(bet)_8(H_2O)_4]^{6+}$ cation and two bistriflimide anions linked by hydrogen bonding.

When complex **1** is kept at 50 °C overnight in a vacuum oven, the melt crystallizes as $[Eu_2(bet)_8(H_2O)_2][Tf_2N]_6{\cdot}2H_2O$. This complex, denoted as **2**, has lost two coordinating water molecules from its first coordination sphere, but these water molecules remain incorporated in the crystal structure as co-crystallized water molecules. The crystal structure of **2** consists of $[Eu_2(bet)_8(H_2O)_2]^{6+}$ cations and six bistriflimide counterions. Figure 2 shows that the two europium(III) ions in the $[Eu_2(bet)_8(H_2O)_2]^{6+}$ cation are linked in a similar way as in the $[Eu_2(bet)_8(H_2O)_4]^{6+}$ cation of compound **1**, namely, by two μ_2-bridging betaine carboxylate groups and two chelating bridging betaine ligands. However, in complex **2**, each europium(III) ion is further surrounded by one monodentate coordinating betaine ligand, one bidentate coordinating betaine ligand, and one water molecule. Thus, instead of two peripheral monodentate betaine ligands and two water

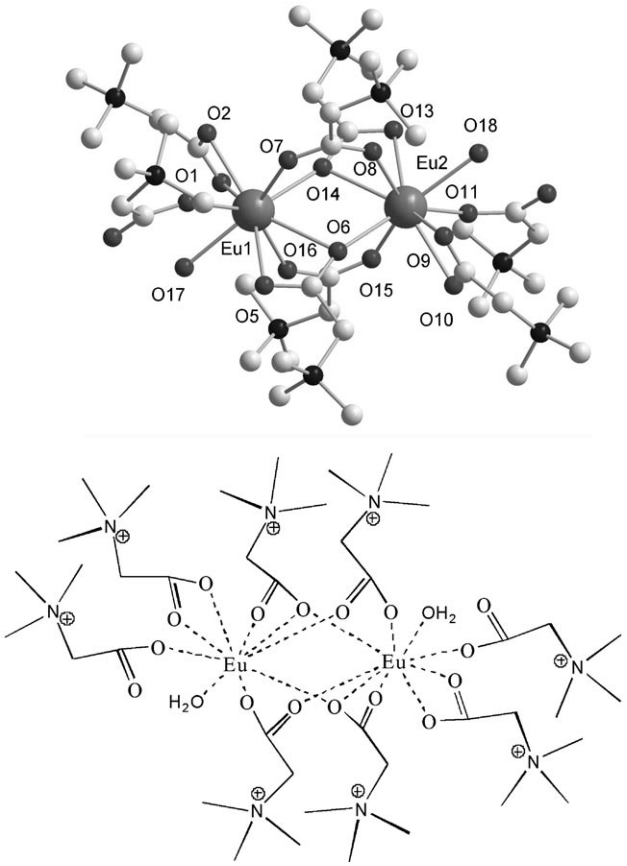

Figure 2. Top: Crystal structure of $[Eu_2(bet)_8(H_2O)_2][Tf_2N]_6 \cdot 2H_2O$ (**2**); hydrogen atoms are omitted for clarity. Bottom: Schematic representation of the $[Eu_2(bet)_8(H_2O)_2]^{6+}$ cation.

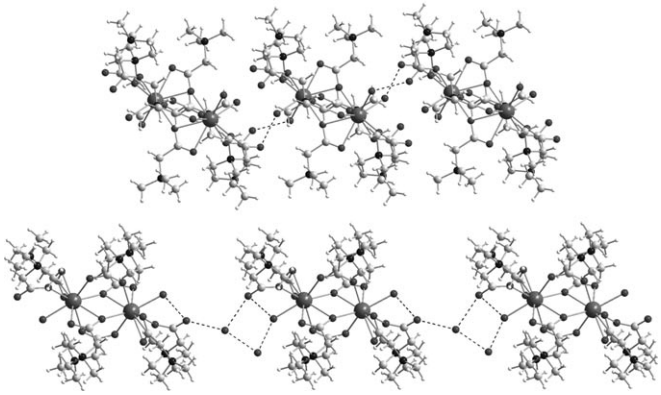

Figure 3. Interlinkage of the dimers by hydrogen bonding in the packing of the crystal structure of **1** (top) and **2** (bottom).

molecules, compound **2** has lost one peripheral water molecule (from the first coordination sphere of each europium(III) ion), and one monodentate betaine ligand has changed its coordination mode from monodentate to bidentate. The coordination number of the europium(III) ions therefore remains nine and the coordination polyhedron can be described as a distorted three-capped trigonal prism. The Eu1–O (carboxylate) bond lengths range from 2.357(3) to 2.634(3) Å. The Eu1–O (aqua) bond length is 2.458(5) Å. The nonequivalent Eu2 center has slightly different bond lengths ranging from 2.362(3) to 2.573(3) Å (carboxy) and 2.476(5) Å (aqua). Two noncoordinating water molecules are present in the crystal structure—one water molecule forms a hydrogen bond with one of the coordinating water molecules (O···O distance of 2.779(8) Å) and the other water molecule bridges two monodentately coordinating betaine ligands of different Eu dimers (O···O distances of 2.802(6) and 2.827(6) Å), linking the dimers together in the crystal packing. Additionally, these two "crystal water" molecules are hydrogen bonded to each other (O···O distance of 2.712(8) Å). The arrangement of the dimers linked by hydrogen bonding is shown in Figure 3 (bottom).

The Eu···Eu distance of the dimeric cation is equal to 4.021(1) Å. There are intramolecular hydrogen bonds between the two terminal coordinating water molecules and monodentate coordinating betaine ligands with O···O distances of 2.688(6) and 2.700(6) Å.

The central metal ion in compounds **1** and **2** is europium(III), a rather large lanthanide ion in comparison with the heavier lanthanide ions such as holmium(III) or erbium(III), which have smaller ionic radii, because of the so-called "lanthanide contraction". The central metal ion in $[Y_2(bet)_6(H_2O)_4][Tf_2N]_6$ (**3**; Figures 4 and 5) is yttrium(III), a rare-

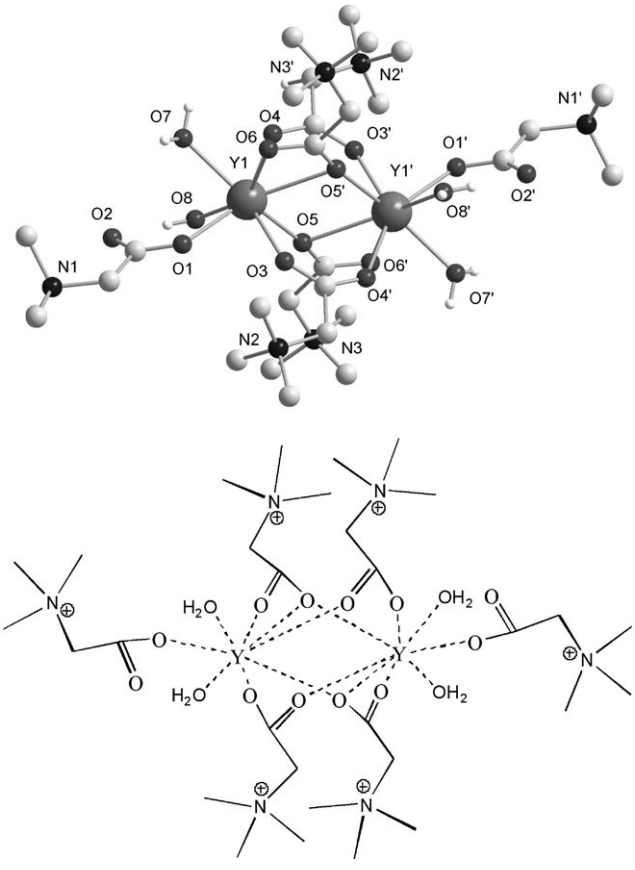

Figure 4. Top: Crystal structure of $[Y_2(bet)_6(H_2O)_4][Tf_2N]_6$ (**3**); hydrogen atoms are omitted for clarity. Bottom: Schematic representation of the $[Y_2(bet)_6(H_2O)_4]^{6+}$ cation.

earth ion with an ionic radius comparable to that of holmium(III) or erbium(III). The crystal structure of $[Y_2(bet)_6(H_2O)_4][Tf_2N]_6$ is also composed of a dimeric cation ($[Y_2(bet)_6(H_2O)_4]^{6+}$) and six bistriflimide anions. In contrast to the europium(III) betaine bistriflimide complexes **1** and **2**, the yttrium complex **3** contains a core cation that is surrounded by only six rather than eight betaine ligands. Because of the inversion center, there is just one crystallographically independent yttrium site present in the structure. The bridging betaine ligands exhibit the same μ_2-bridging and chelating bridging coordination mode as for the respective europium(III) compounds. Furthermore, each yttrium(III) ion is coordinated by two monodentate coordinating betaine ligands and two water molecules, which results in an eight-coordinate environment of yttrium(III) in a distorted square antiprismatic geometry. The Y–O (carboxylate) bond lengths range from 2.245(2) to 2.427(2) Å. The Y–O (aqua) bond lengths are 2.336(3) and 2.343(2) Å. The Y—Y distance of the dimeric cation is 3.857(1) Å. There is hydrogen bonding (Figure 5) from the two coordinating water molecules to three bistriflimide anions with O···O distances ranging from 2.734(4) to 2.865(9) Å. An intramolecular hydrogen bond is observed from the monodentate coordinating betaine ligand to an aqua ligand with an O···O distance of 2.666(4) Å.

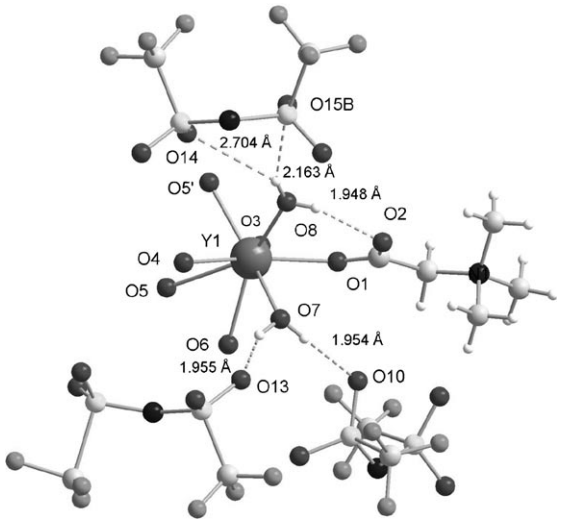

Figure 5. Hydrogen bonding in the crystal structure of **3**.

The crystallographic data of compounds **1–3** are summarized in Table 1.

Table 1. Summary of the crystallographic data of **1**, **2**, and **3**.

	1	**2**	**3**
formula	$C_{52}H_{88}Eu_2F_{36}N_{14}O_{44}S_{12}$	$C_{52}H_{88}Eu_2F_{36}N_{14}O_{44}S_{12}$	$C_{42}H_{74}F_{36}N_{12}O_{40}S_{12}Y_2$
M_r	2986.14	2986.13	2633.79
dimensions [mm^3]	$0.2\times0.1\times0.1$	$0.35\times0.2\times0.15$	$0.4\times0.25\times0.2$
crystal system	triclinic	monoclinic	triclinic
space group	$P\bar{1}$ (No. 2)	$P2_1$ (No. 4)	$P\bar{1}$ (No. 2)
a [Å]	10.3241(19)	14.1945(8)	10.4118(3)
b [Å]	17.910(3)	24.2149(17)	15.4634(5)
c [Å]	30.624(6)	15.7258(9)	15.7177(4)
α [deg]	90.178(12)	90	104.752(2)
β [deg]	93.708(13)	95.681(4)	97.841(2)
γ [deg]	98.507(12)	90	90.535(2)
V [Å^3]	5587.8(18)	5378.7(6)	2421.7(1)
Z	2	2	1
ρ_{calcd} [g cm^{-3}]	1.775	1.844	1.806
$\mu_{Cu_{K\alpha}}$ [mm^{-1}]	11.385	11.828	5.460
absorption correction	multiscan	refined from ΔF	multiscan
$F(000)$	2984	2984	1324
T [K]	298	100	100
measured rflns	52170	41267	22973
unique rflns	19132	10227	8811
obs. rflns ($I_0>2\sigma(I_0)$)	9596	9214	7428
parameters refined	1631	1466	871
goodness-of-fit on F^2	1.112	0.997	1.044
R_1	0.0913	0.0464	0.0478
wR_2	0.1721	0.1089	0.1165
R_1(all data)	0.1839	0.0525	0.0585
wR_2(all data)	0.2061	0.1122	0.1224

Luminescence spectroscopy: As already mentioned in the introduction, the trivalent europium ion can be used to probe the local symmetry around the metal ion. To correlate the spectroscopic fine structure to coordination symmetry in our betaine complexes, compound **1** was used as a reference material by recording the luminescence spectrum of this complex as a pure powder at 77 K. Direct excitation of the europium(III) ion in the $^5L_6$ level at 393 nm (25445 cm^{-1}) resulted in the observation of the typical red europium(III)-centered luminescence (Figure 6). The electronic transitions corresponding to the peaks in the spectrum are indicated in Table 2. They all originate from the $^5D_0$ excited state of the europium(III) ion and decay towards the different J levels of the ^7F term (^7F_J, $J=0$, 1, 2, 3, and 4; transitions towards $^7F_5$ and $^7F_6$ correspond to wavelengths that are located in the near-infrared region, where the detector used has no sensitivity.). The peak at the highest energy in the spectrum corresponds to the $^5D_0\rightarrow{}^7F_0$ transition. This transition, originating from a nondegenerate excited state and going to a nondegenerate ground state, can consist of a maximum of one peak. The observation of more than one peak in this spectral region indicates the presence of more than one crystallographically independent europium(III) site.

Figure 7 shows an enlarged view of the peak corresponding to the $^5D_0\rightarrow{}^7F_0$ transition in the luminescence spectrum of compound **1**. The shape of the peak can be fitted with one Gaussian function, indicated as the dotted line and located at 17245 cm^{-1}, suggesting that only one crystallographically independent europium(III) site is present in the

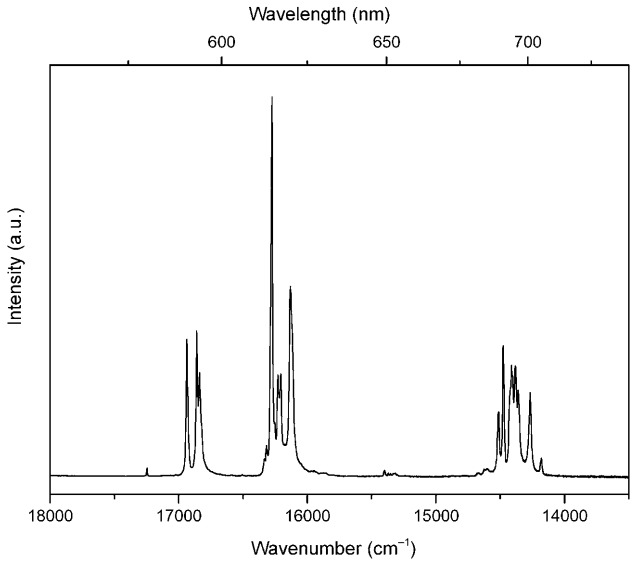

Figure 6. Luminescence spectrum of **1** in the solid state recorded at 77 K; $\lambda_{ex}=393$ nm.

Table 2. Summary of the transitions observed in the luminescence spectrum of **1** in the solid state recorded at 77 K; $\lambda_{ex}=393$ nm.

Line assignment	$\tilde{\nu}$ [cm^{-1}]	λ [nm]	$I(^5D_0\rightarrow{}^7F_J)/I(^5D_0\rightarrow{}^7F_1)$
$^5D_0\rightarrow{}^7F_0$	17245	580	0.01
$^5D_0\rightarrow{}^7F_1$	16860	593	1.00
$^5D_0\rightarrow{}^7F_2$	16275	614	2.42
$^5D_0\rightarrow{}^7F_3$	15400	650	0.04
$^5D_0\rightarrow{}^7F_4$	14475	691	1.82

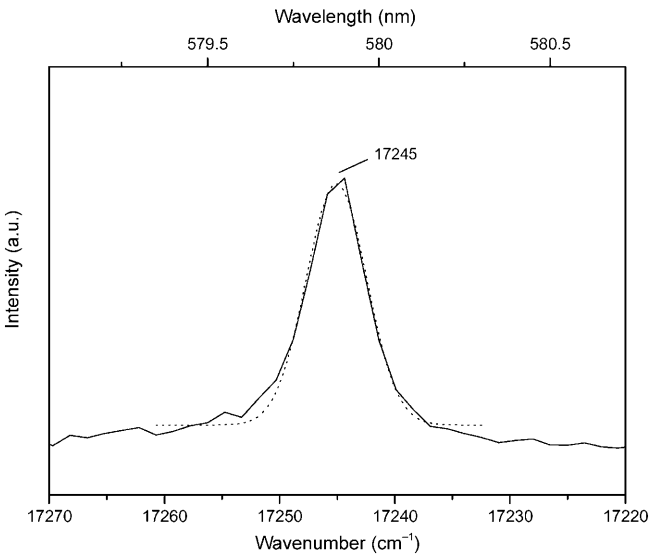

Figure 7. Detail of the luminescence spectrum of **1**, showing the peak corresponding to the $^5D_0\rightarrow{}^7F_0$ transition. Experimental data shown as solid line; fit shown as dotted line.

compound. However, from the crystal structure we learned that although the europium(III) ions present within one dimeric unit are indeed identical, two slightly independent dimeric units are present in the asymmetric unit. Nevertheless, the local symmetry of the first coordination sphere clearly does not differ significantly enough to result in more than one peak for the $^5D_0\rightarrow{}^7F_0$ transition in the spectrum or broadening of this peak. Indeed, even though the Eu···Eu distances in the crystallographically independent dimers in this compound are slightly different, the local surroundings of the Eu^{III} ions are virtually the same.

The second peak (or set of peaks) in the spectrum corresponds to the $^5D_0\rightarrow{}^7F_1$ transition. Being a magnetic dipole transition, its intensity is more or less independent of the local surrounding of the europium(III) ion. Only a maximum of three peaks can account for this transition, which is indeed the number of peaks for the $^5D_0\rightarrow{}^7F_1$ transition observed in the spectrum. This result means that the local symmetry of the first coordination sphere around the europium(III) ion is either orthorhombic, monoclinic, or triclinic. One can distinguish between these point groups by analyzing the peak corresponding to the $^5D_0\rightarrow{}^7F_2$ transition, which can be maximally split in five crystal-field components.[58] As shown in Figure 6, indeed a splitting in five peaks for this transition is observed, indicating a local symmetry of C_1, C_2, or C_s. Investigation of the crystal structure indeed reveals a local symmetry which is close to C_2. Furthermore, the $^5D_0\rightarrow{}^7F_2$ transition is a so-called "hypersensitive" transition, which means that the intensity of the peak associated with this transition is strongly dependent on the local environment of the europium(III) ion. The ratio between the intensities $I(^5D_0\rightarrow{}^7F_2)/I(^5D_0\rightarrow{}^7F_1)$ of the peaks associated with the $^5D_0\rightarrow{}^7F_2$ and the $^5D_0\rightarrow{}^7F_1$ transitions therefore serves as a sensitive indicator of subtle changes in the coordination environment of the europium(III) ion.

Table 2 gives the intensity ratios for the different $^5D_0\rightarrow{}^7F_J$ transitions with respect to the magnetic dipole transition $^5D_0\rightarrow{}^7F_1$. The luminescence decay curve for compound **1**, recorded at 77 K, could be fitted with a biexponential function, corresponding to decay times of (456 ± 2) (92%) and (1142 ± 92) μs (8%). At room temperature, the decay is monoexponential, corresponding to a decay time of (400 ± 4) μs.

When compound **1** is thoroughly dried at 50°C in a vacuum oven overnight, it is converted into compound **2**, which has lost two water molecules from the first coordination sphere (one for each europium(III) ion). Figure 8 shows the luminescence spectrum of compound **2** recorded at 77 K as the pure powder for direct excitation of the europium(III) ion at 393 nm (25445 cm^{-1}). This spectrum is clearly different from the one shown in Figure 6, which is in accordance with the structural change induced by the drying process. A closer look at the $^5D_0\rightarrow{}^7F_0$ line (Figure 9) reveals the presence of a shoulder in this line, which can be fitted by two Gaussian curves: one centered at 17245 cm^{-1} and another one at 17240 cm^{-1}. We find that the differences between the europium(III) sites in compound **2** are more pronounced than those in compound **1**, where the europium(III) sites are virtually identical. Further inspection of the fine structure in the spectrum in Figure 8 indicates a low

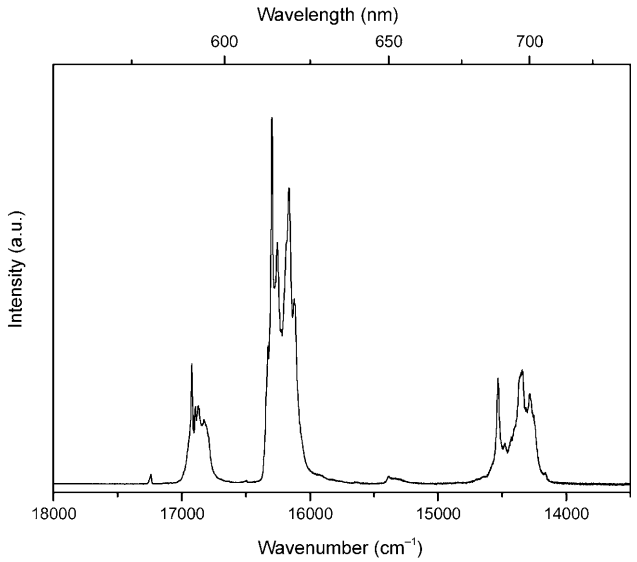

Figure 8. Luminescence spectrum of **2** in the solid state recorded at 77 K; $\lambda_{ex}=393$ nm.

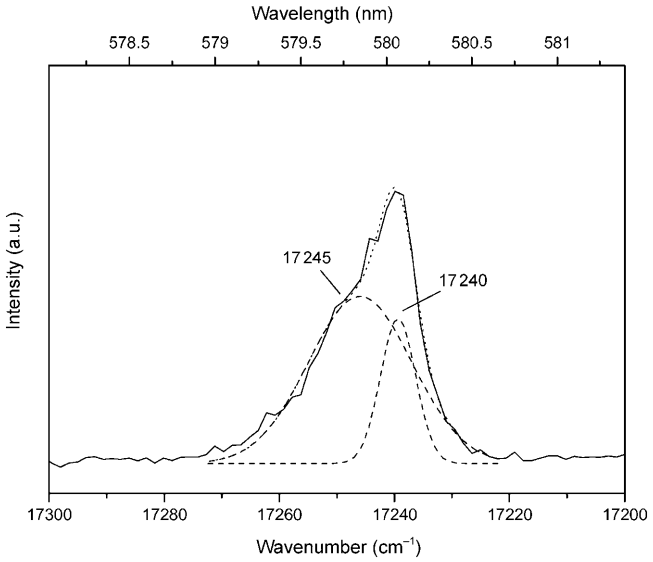

Figure 9. Detail of the luminescence spectrum of **2**, showing the peak(s) corresponding to the $^5D_0\rightarrow{}^7F_0$ transition. Experimental data shown as solid line; fit of two maxima shown as dashed lines; sum of the dashed lines shown as dotted line.

symmetry of the first coordination sphere around the europium(III) ions in compound **2**. Of course, the splitting of the peak corresponding to the $^5D_0\rightarrow{}^7F_0$ transition also indicates that more than three peaks can be present for the $^5D_0\rightarrow{}^7F_1$ transition, owing to overlapping spectra and similarly more than five peaks can be present for the $^5D_0\rightarrow{}^7F_2$ transition.

Table 3 gives the intensity ratios for the different $^5D_0\rightarrow{}^7F_J$ transitions with respect to the magnetic dipole transition $^5D_0\rightarrow{}^7F_1$ in Figure 8. The ratio between the intensities of the $^5D_0\rightarrow{}^7F_2$ transition and the $^5D_0\rightarrow{}^7F_1$ transition equals 4.22, compared with 2.42 for compound **1**, indicating significant

Table 3. Summary of the transitions observed in the luminescence spectrum of **2** in the solid state recorded at 77 K; $\lambda_{ex}=393$ nm.

Line assignment	$\tilde{\nu}$ [cm^{-1}]	λ [nm]	$I(^5D_0\rightarrow{}^7F_J)/I(^5D_0\rightarrow{}^7F_1)$
$^5D_0\rightarrow{}^7F_0$	17240	580.0	0.02
$^5D_0\rightarrow{}^7F_1$	16920	591.0	1.00
$^5D_0\rightarrow{}^7F_2$	16295	615.0	4.22
$^5D_0\rightarrow{}^7F_3$	15380	650.0	0.08
$^5D_0\rightarrow{}^7F_4$	14345	695.0	1.88

structural differences. The luminescence decay curve for compound **2** recorded at 77 K could be fitted with a biexponential function, corresponding to decay times of (657 ± 40) (61%) and (1225 ± 142) μs (39%). At room temperature, the decay is monoexponential, corresponding to a decay time of (650 ± 10) μs. The fact that the luminescence decay times are clearly longer in compound **2** than those in compound **1** can also be explained by the presence of two rather than four water molecules in the first coordination sphere of the europium(III) ion. Water molecules are known to be efficient quenchers of the excited state in trivalent lanthanide ions, owing to the O–H vibrations, which couple to the lanthanide's energy levels (energy gap law).[84] It should be noted that drying compound **1** overnight at 50 °C without applying a vacuum did not result in any significant change in the luminescence spectrum. This result indicates that the drying needs to be done in vacuo to remove the water molecules from the first coordination sphere of the europium(III) ions.

The findings described above indicate that the europium(III) luminescence spectrum can be used to distinguish between different europium(III) coordination compounds, on the condition that significant changes in the first coordination sphere take place. In theory, however, one would not be able to distinguish between a dimeric compound in which the two europium(III) ions are equivalent (such as compound **1**, assuming negligible differences between the europium(III) ions in this compound), and the individual monomers, resulting from the splitting of this dimer, if the coordination symmetry in the monomers is the same as that in the dimer. However, splitting of dimeric compound **2** into monomers should result in a change in the luminescence spectrum, providing the monomers each have the same symmetry (otherwise one would have a mixture, which would again complicate the interpretation of the spectrum): the shoulder in the $^5D_0\rightarrow{}^7F_0$ line should disappear.

When compound **1** is dissolved in the ionic liquid [Hbet][Tf_2N], the resulting solution vitrifies upon cooling to 77 K, allowing spectroscopic investigation at low temperature. Figure 10 shows the luminescence spectrum of the resulting vitrified sample excited at 393 nm (25445 cm^{-1}). Closer inspection of the $^5D_0\rightarrow{}^7F_0$ transition reveals only a single peak, suggesting the breakdown of the dimer into two indistinguishable monomers. However, the luminescence decay curve recorded at 77 K shows a clear biexponential pattern, with components (203 ± 37) (37%) and (537 ± 30) μs (63%). Normally, a well-defined monomeric europium(III) complex

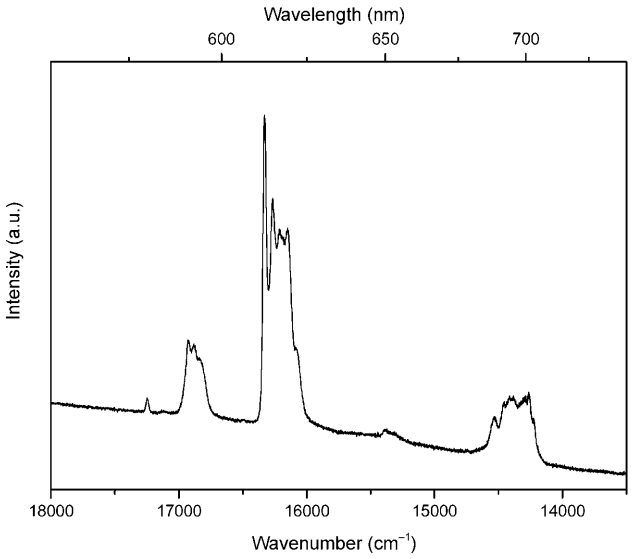

Figure 10. Luminescence spectrum of **1** dissolved in the ionic liquid [Hbet][Tf_2N] recorded at 77 K in a vitrified state; $\lambda_{ex}=393$ nm.

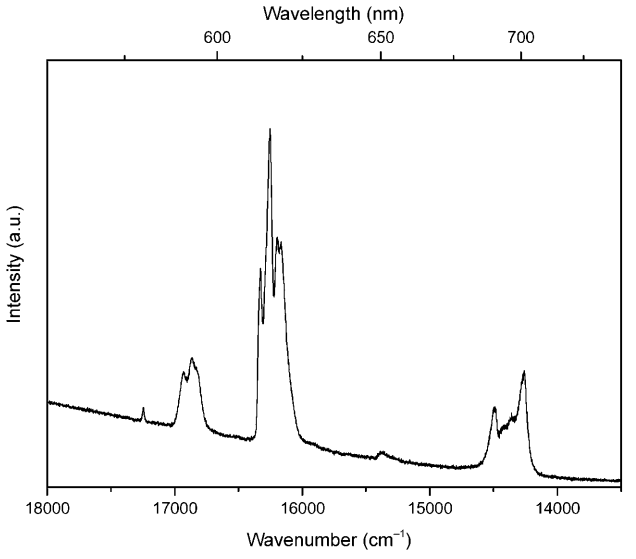

Figure 11. Luminescence spectrum of **1** dissolved in the ionic liquid [C_4mim][Tf_2N] recorded at 77 K in a vitrified state; $\lambda_{ex}=393$ nm.

would be expected to have a monoexponential decay curve. At room temperature, the decay curve can be fitted with components (188 ± 76) (25%) and (451 ± 95) μs (75%). Table 4 gives the intensity ratios for the different $^5D_0\rightarrow{}^7F_J$ transitions with respect to the magnetic dipole transition $^5D_0\rightarrow{}^7F_1$ in Figure 10. The ratio between the intensities of the $^5D_0\rightarrow{}^7F_2$ transition and the $^5D_0\rightarrow{}^7F_1$ transition equals 4.56.

Table 4. Summary of the transitions observed in the luminescence spectrum of **2** dissolved in the ionic liquid [Hbet][Tf_2N] recorded at 77 K (vitrified sample); $\lambda_{ex}=393$ nm.

Line assignment	$\tilde{\nu}$ [cm^{-1}]	λ [nm]	$I(^5D_0\rightarrow{}^7F_J)/I(^5D_0\rightarrow{}^7F_1)$
$^5D_0\rightarrow{}^7F_0$	17250	580.0	0.04
$^5D_0\rightarrow{}^7F_1$	16930	590.5	1.00
$^5D_0\rightarrow{}^7F_2$	16330	612.5	4.56
$^5D_0\rightarrow{}^7F_3$	15370	650.5	0.16
$^5D_0\rightarrow{}^7F_4$	14265	701.0	1.70

Dissolution of compound **1** in the ionic liquid [C_4mim][Tf_2N] also results in a solution, which can be vitrified upon cooling to 77 K. The luminescence spectrum obtained from this vitrified sample is shown in Figure 11. It shows a rather strong background fluorescence from the imidazolium group of the ionic liquid. Nevertheless, the europium(III)-centered luminescence transitions can be clearly distinguished, revealing a single peak for the $^5D_0\rightarrow{}^7F_0$ transition. The luminescence decay curve recorded at 77 K shows a biexponential pattern with components (392 ± 26) (31%) and (813 ± 22) μs (69%). At room temperature, these values are (544 ± 30) (19%) and (1013 ± 10) μs (81%). The ratio between the intensities of the $^5D_0\rightarrow{}^7F_2$ transition and the $^5D_0\rightarrow{}^7F_1$ transition equals 4.33, as can be seen in Table 5.

Table 5. Summary of the transitions observed in the luminescence spectrum of **2** dissolved in the ionic liquid [C_4mim][Tf_2N] recorded at 77 K (vitrified sample); $\lambda_{ex}=393$ nm.

Line assignment	$\tilde{\nu}$ [cm^{-1}]	λ [nm]	$I(^5D_0\rightarrow{}^7F_J)/I(^5D_0\rightarrow{}^7F_1)$
$^5D_0\rightarrow{}^7F_0$	17245	580.0	0.03
$^5D_0\rightarrow{}^7F_1$	16865	593.0	1.00
$^5D_0\rightarrow{}^7F_2$	16250	615.0	4.33
$^5D_0\rightarrow{}^7F_3$	15365	651.0	0.07
$^5D_0\rightarrow{}^7F_4$	14260	701.0	1.79

In conclusion, clear changes in the luminescence spectrum of compound **1** occur upon dissolution in the ionic liquids [Hbet][Tf_2N] and [C_4mim][Tf_2N], but ultimately luminescence spectroscopy alone cannot unequivocally discriminate between dimeric and monomeric europium(III) betaine complexes and, as such, it remains unclear whether the dimeric compound **1** stays intact upon dissolution in the ionic liquids [Hbet][Tf_2N] and [C_4mim][Tf_2N] or if it dissociates into monomers.

NMR spectroscopy: Nuclear magnetic resonance (NMR) studies were performed on the yttrium(III) compound **3** in the [Hbet][Tf_2N] ionic liquid to gain additional insight into the nature of the complex present in solution. ^{89}Y NMR spectroscopy has been proven to be a useful tool for probing solution dynamics of yttrium compounds.[85] Advantages of the ^{89}Y nucleus are its high abundance and spin $I=1/2$, but the negative magnetic moment, low sensitivity, and very long relaxation times usually impede the observation of ^{89}Y NMR signals. The ^{89}Y NMR spectrum of $[Y_2(bet)_6(H_2O)_4][Tf_2N]_6$ dissolved in [Hbet][Tf_2N] was recorded at 363 K and shows only a single resonance at $\delta=37.7$ ppm. This result implies the presence of one yttrium(III) site or two equivalent yttrium(III) sites in solution. The data are

not sufficient to discriminate between a dimeric and a monomeric complex, since the symmetric dimeric structure is also expected to give a single ^{89}Y NMR resonance. ^{1}H and ^{13}C NMR spectra of the same solution showed only one set of resonances that could be unambiguously assigned to the betaine anion. Interestingly, the carbonyl resonance in the ^{13}C NMR spectrum detected at 313 K showed a broad resonance ($\nu_{1/2}=73$ Hz) at $\delta=169.8$ ppm. Heating the sample to 353 K resulted in sharpening of this resonance ($\nu_{1/2}=39$ Hz) and its shifting to $\delta=170.7$ ppm (Figure 12). This result indicates that there is dynamic exchange in the system, which becomes faster at elevated temperatures. The dynamic process most likely involves the exchange between the betaine anions of the ionic liquid and the betaine ligands coordinated to the yttrium(III) ion, corresponding to an equilibrium between dimers and monomers in solution.

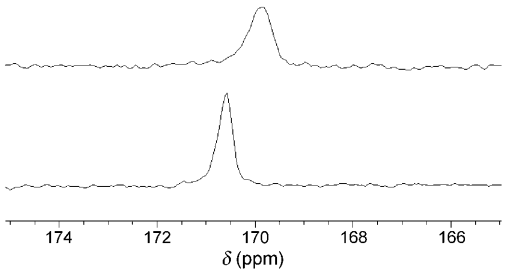

Figure 12. ^{13}C NMR signal of the carbonyl resonance of the solution containing **3** dissolved in the [Hbet][Tf_2N] ionic liquid recorded at 313 K (top) and 353 K (bottom).

EXAFS: The pure compound **2** was investigated by X-ray absorption spectroscopy. The known dimeric structure of this compound was chosen to serve as a "standard", allowing the extraction of structural parameters such as Debye–Waller factors. Moreover, we expected to see the Eu···Eu interaction in the Fourier-transformed EXAFS spectrum. This would allow us to distinguish between dimeric and monomeric compounds, yielding crucial structural information about the betaine complexes upon dissolution in the ionic liquids [Hbet][Tf_2N] and [C_4mim][Tf_2N].

The identification of dimeric compounds by EXAFS requires either heavy scatterers (for example, actinide ions such as the uranyl ion, UO_2^{2+}), short absorber–scatterer distances, or low structural disorder. Although the europium(III) ion is quite a heavy ion, the low coordination number (each europium(III) ion in the dimer only "sees" one other europium(III) ion) generates only a relatively weak backscattered Eu···Eu signal. Furthermore, the Eu···Eu distance of 4.0217(12) Å in compound **2** is rather large, because of the bridging coordination mode of the betaine carboxylate groups. The structural disorder is expressed through the Debye–Waller factors, which contain two parts: a long-range structural parameter, which is an inherent property of the material under investigation, and a thermal disorder parameter, related to the thermal vibration of all the atoms in the molecule. This thermal disorder parameter can be "frozen" out by measuring the EXAFS spectrum at low temperature. In our experiment, we used an Oxford Instruments closed cycle helium cryostat, allowing measurements at temperatures as low as 13 K.

Figure 13 shows the raw k^3-weighted EXAFS spectrum and the Fourier transform of the pure compound **2**, diluted with boron nitride and pressed in a pellet, measured at 13 K. The spectrum is more noisy at higher k values, resulting in a relatively high noise level in the Fourier-transformed spectrum as well. The k range is limited to about $k=12$ Å^{-1} because of the presence of the europium L_{II} edge. The Fourier-transformed spectrum is dominated by a dis-

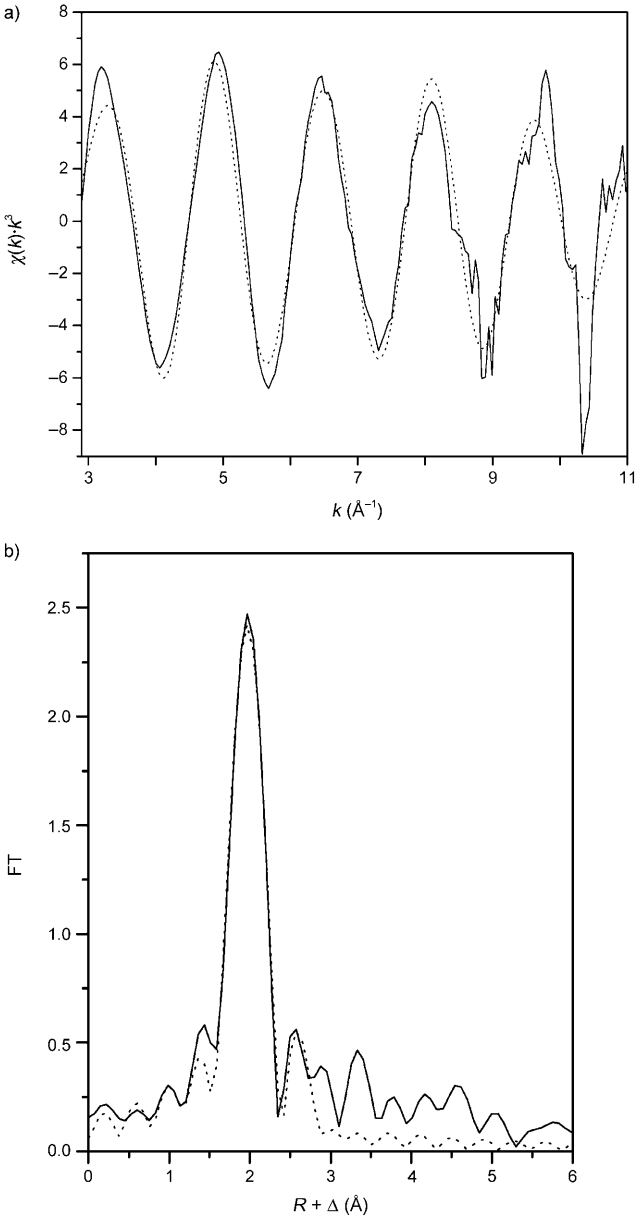

Figure 13. Raw k^3-weighted EXAFS spectrum (a) and Fourier-transformed spectrum (b) of **2** recorded at 13 K. Experimental data are shown as the solid curve, whereas fitted data are shown as the dotted line.

tinct peak at $R+\Delta=2$ Å, corresponding to the oxygen shell surrounding the two europium(III) ions. The peaks in the Fourier-transformed spectrum were not corrected for the phase shift. The most important scattering paths of the photoelectron are listed in Table 6. These were derived from the crystal structure of compound **2** shown in Figure 2.

Table 6. Main scattering paths of the photoelectron, as derived for $[Eu_2(bet)_8(H_2O)_2][Tf_2N]_6$.

Scattering path	Distance [Å]	Amplitude
Eu···O	2.286	100
Eu···O	2.646	64.7
Eu···C	2.835	50.6
Eu···C	3.402	30.2
Eu···Eu	4.022	39.3
Eu···O···C	3.480	65.0
Eu···O···C···O	3.559	243
Eu···C···O···C	4.674	16.2

The dominating peak in the Fourier-transformed spectrum can be fitted by a single oxygen shell, resulting in a coordination number N of eight oxygen atoms (per europium(III) ion) and a real Eu–O distance R of 2.37 Å (Debye–Waller factor $\sigma^2=0.0040$ Å^2, $\Delta E=4.4$ eV). Including additional Eu–C, Eu···Eu, or multiple scattering paths did not result in physically meaningful results. No distinguishable peak at a real distance of 4 Å could be found. Therefore, one has to conclude that EXAFS alone cannot give sufficient structural insight in the coordination geometry of the $[Eu_2(bet)_8(H_2O)_2]^{6+}$ unit to distinguish between dimers and monomers. As a result, no attempts were made to interpret EXAFS data from the solutions of $[Eu_2(bet)_8(H_2O)_2][Tf_2N]_6\cdot 2H_2O$ in the ionic liquids.

HEXS: To resolve this problem, we used high-energy X-ray scattering (HEXS). Whereas EXAFS probes exclusively the scattering pairs in the vicinity of an excited atom, HEXS reveals all scattering pairs in solution. Furthermore, HEXS is more sensitive to longer distances than EXAFS. As a result, a single scattering pair with heavy atoms such as the Eu dimer may dominate the signal.

First, we subjected the pure compound **2** to a HEXS measurement to see whether the Eu···Eu scattering pair could be distinguished. Next, a solution of **2** in the ionic liquid [Hbet][Tf_2N] was investigated. If the dimeric structure were to be preserved in solution, a related Eu···Eu scattering peak should occur. To make sure the relatively weak Eu···Eu scattering pair could be distinguished in the solution, we used a concentration of 500 mM Eu, corresponding to a fourfold dilution relative to the crystalline compound **2**. These samples were then compared with the pure ionic liquid [Hbet][Tf_2N]. Figure 14 shows the extracted reduced structure function $S(Q)$ to a value of $Q=11$ Å^{-1}. The extracted reduced structure functions for the three samples show some differences. Besides a series of Bragg reflections, the crystalline dimer shows a remarkable background from submicrometer-sized material generating a signal similar to that of the liquids.

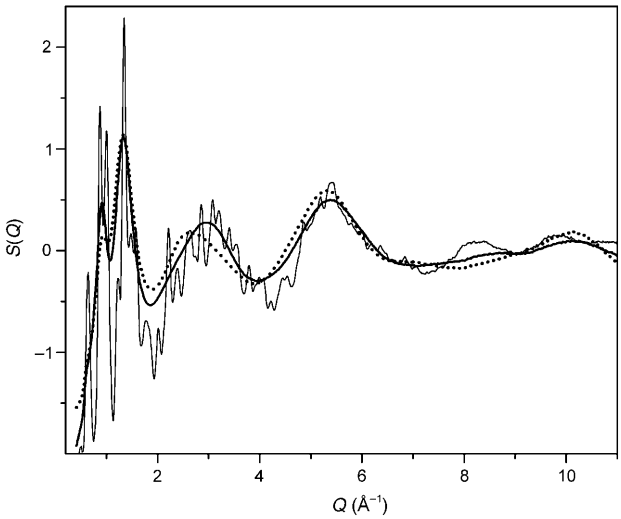

Figure 14. Extracted reduced structure functions $S(Q)$ obtained from HEXS measurements on **2** in the crystalline form (thin solid line), **2** dissolved in the ionic liquid [Hbet][Tf_2N] (thick solid line), and the pure ionic liquid [Hbet][Tf_2N] (dotted line).

For the subsequent Fourier-transformed spectrum shown in Figure 15, $S(Q)$ data up to $Q=16.5$ Å^{-1} were used. The first peak of the crystalline dimer originates predominantly from the S–O distances between 1.373 and 1.444 Å, resulting in an average peak at 1.42 Å. This distance is dominant in the crystal structure as well as in the ionic liquid. The second peak shows some important differences between the Eu complex **2** and the ionic liquid. In the crystalline dimer, there is a variety of distances contributing to the peak at 2.50 Å, but the main contributions are due to the Eu–O distances ranging from 2.357 to 2.634 Å and the S–F distances

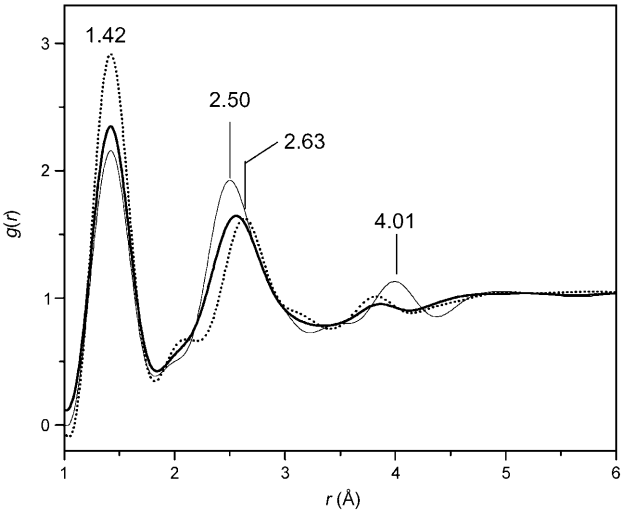

Figure 15. Pair distribution functions $g(r)$ obtained from the reduced structure functions in Figure 14. (Crystalline form of **2** (thin solid line), **2** dissolved in the ionic liquid [Hbet][Tf_2N] (thick solid line), and the pure ionic liquid [Hbet][Tf_2N] (dotted line)).

ranging from 2.584 to 2.634 Å. It should be noted that the second peak in the [Hbet][Tf_2N] spectrum occurs at 2.63 Å, revealing a center of gravity at a significantly longer distance. This peak is mainly due to the S–F distances ranging from 2.587 and 2.624 Å. The distance, represented by the corresponding peak from the solution of the Eu dimer **2** in [Hbet][Tf_2N], occurs in between these two distances.

The signal from the crystalline Eu dimer **2** shows a significant peak with an Eu···Eu distance of 4.01 Å. This distance corresponds well (±0.01 Å) to the value obtained from the single-crystal diffraction. This peak does not occur in the signal from the pure [Hbet][Tf_2N] sample, nor does it appear in the signal from the solution of the Eu dimer **2** in [Hbet][Tf_2N] in the expected intensity ratio (corresponding to fourfold dilution). This result strongly suggests that the solution is dominated by monomers, although these monomers could be in equilibrium with a very small number of dimers (too small to be distinguished).

It should be remarked that the solution studied by HEXS is still 200 times more concentrated than those studied by luminescence spectroscopy (500 mM versus 2.5 mM), but it seems reasonable to assume that the higher dilution would shift the possible equilibrium between monomers and dimers in solution even further towards the monomers.

Conclusions

A combination of luminescence spectroscopy, ^{1}H, ^{13}C, and ^{89}Y NMR spectroscopy, and the synchrotron techniques EXAFS and HEXS were applied to gain insight in the speciation of rare-earth bistriflimide complexes in the ionic liquids [Hbet][Tf_2N] and [C_4mim][Tf_2N].

Europium(III) luminescence spectroscopy proved to be a powerful tool to distinguish between europium(III) ions with significantly different local coordination geometries, clearly indicating changes in the spectrum upon dissolution of the dimeric compounds in the ionic liquids, but it failed to unequivocally distinguish between the presence of dimers or monomers in solution.

Although ^{89}Y NMR spectroscopy was inconclusive in distinguishing between the monomeric or dimeric nature of the dissolved complex, variable-temperature ^{13}C NMR spectroscopy indicated the presence of a dynamic process in solution that most likely involves the exchange between the betaine anions of the ionic liquid and the coordinated betaine ligands and as a result may point towards an equilibrium between dimers and monomers in solution.

EXAFS spectroscopy is a valuable technique to probe the first coordination shells of metal ions, but in this case, it is relatively insensitive for features that are located at longer distances and hence we could not observe the Eu···Eu backscattering, even in the crystalline dimeric materials.

Finally, HEXS indicated the decomposition of the europium(III) dimer upon dissolution in the ionic liquid [Hbet][Tf_2N].

This work illustrates the fact that a carefully chosen combination of complementary analytical techniques, including synchrotron techniques, can provide valuable and crucial information on the speciation of f-block element coordination compounds in ionic liquids.

Experimental Section

Chemicals: All commercially available reagents and starting materials were used without further purification unless otherwise stated. Eu_2O_3 and Y_2O_3 were purchased from ACROS (Belgium). Li(Tf_2N) was purchased from IoLiTec (Germany).

Synthesis of the ionic liquid [Hbet][Tf_2N]: The ionic liquid [Hbet][Tf_2N] was synthesized by using a procedure described earlier.[48] An aqueous solution of betainium hydrochloride (1 mol, 153.61 g dissolved in 150 mL of water) was added to an aqueous solution of lithium bis(trifluoromethylsulfonyl)imide (1 mol, 287.08 g dissolved in 300 mL of water). The mixture was stirred for 1 h at room temperature. The ionic liquid phase immediately separated from the aqueous phase after combination of the two aqueous solutions. After separation of the phases, the ionic liquid phase was washed with small amounts of cold water until no chloride impurities could be detected by the silver nitrate test. The ionic liquid was evaporated to dryness at 80 °C in vacuo on a rotary evaporator. ^{1}H NMR (300 MHz, [D_6]DMSO, TMS): $\delta = 4.27$ (s, 2H), 3.19 (s, $3\times CH_3$); ^{13}C NMR (100.62 MHz [D_6]DMSO, TMS): $\delta = 167.38$ (COO), 119.8 (CF_3, q, $J_{CF} = 321.5$ Hz), 64.06 (N–CH_2), 54.16 ($3\times CH_3$); elemental analysis calcd (%) for $C_7H_{12}F_6N_2O_6S_2$ ($M_r = 398.302$): C 21.10, H 3.03, N 7.03; found: C 20.78, H 3.24, N 6.85; IR (NaBr windows, cm^{-1}): 1742s (COOH), 1640w (COO), 1475m (CH_2), 1135m (CH_3).

Synthesis of ionic liquid [C_4mim][Tf_2N]: [C_4mim][Tf_2N] was synthesized by following a synthesis and purification route reported previously to obtain an ionic liquid of optical quality.[86]

Synthesis of [Eu_2(bet)$_8$(H_2O)$_4$][Tf_2N]$_6$: Eu_2O_3 (1 g, 10.75 mmol) was mixed with [Hbet][Tf_2N] (8.57 g, 21.51 mmol) and water (10 mL). The mixture was stirred under reflux for 12 h. The excess of europium(III) oxide was removed by filtration. After filtration, water was evaporated under vacuum. Colorless crystals were obtained after recrystallization of the compound in a small amount of water. Elemental analysis calcd (%) for $C_{52}H_{88}Eu_2F_{36}N_{14}O_{44}S_{12}$ ($M_r = 2986.1$): C 20.92, H 2.97, N 6.57; found C 21.16, H 2.86, N 6.43.

Synthesis of [Eu_2(bet)$_8$(H_2O)$_2$][Tf_2N]$_6$·2H_2O: This compound was synthesized starting from [Eu_2(bet)$_8$(H_2O)$_4$][Tf_2N]$_6$ and drying the compound at 80 °C on a rotary evaporator. Colorless crystals were obtained after the molten compound was left to cool down slowly to room temperature. Elemental analysis calcd (%) for $C_{52}H_{88}Eu_2F_{36}N_{14}O_{44}S_{12}$ ($M_r = 2986.1$): C 20.92, H 2.97, N 6.57; found C 20.79, H 3.05, N 6.71.

Synthesis of [Y_2(bet)$_6$(H_2O)$_4$][Tf_2N]$_6$: Y_2O_3 (1 g, 4.43 mmol) was mixed with [Hbet][Tf_2N] (3.98 g, 10 mmol) and water (10 mL). The mixture was stirred under reflux for 12 h. The excess of yttrium(III) oxide was removed by filtration. After filtration, water was evaporated under vacuum. Colorless crystals were obtained after recrystallization of the compound in a small amount of water. Elemental analysis calcd (%) for $C_{42}H_{74}F_{36}N_{12}O_{40}S_{12}Y_2$ ($M_r = 2633.79$): C 13.15, H 1.10, N 12.27; found C 13.36, H 1.34, N 12.43.

Crystallography: X-ray intensity data were collected on a SMART 6000 diffractometer equipped with a CCD detector using Cu-Kα radiation ($\lambda = 1.54178$ Å). The images were interpreted and integrated with the program SAINT from Bruker.[87] All three structures were solved by direct methods and refined by full-matrix least-squares analysis on F^2 using the SHELXTL program package.[88] Non-hydrogen atoms were anisotropically refined, and the hydrogen atoms in the riding mode with isotropic temperature factors were fixed at 1.2 times U(eq) of the parent atoms (1.5 times for methyl groups). For compound **3**, hydrogen atoms H7D, H7E, H8E, and H8D were located in the difference Fourier map and refined unrestrained with isotropic temperature factors fixed at 1.2

times U(eq) of the parent O7 and O8 atoms. CCDC 694410 (**1**), 694411 (**2**), and 694412 (**3**) contain the supplementary crystallographic data for this paper. These data can be obtained free of charge from The Cambridge Crystallographic Data Centre via www.ccdc.cam.ac.uk/data_request/cif. The crystallographic data of the complexes are summarized in Table 1.

Luminescence spectroscopy: Luminescence measurements were performed on an Edinburgh Instruments FS900 spectrofluorimeter equipped with a Xe900 450W xenon arc lamp as the steady-state excitation source, a μF900 pulsed xenon lamp as the time-resolved excitation source, excitation and emission monochromators with 1800 lines mm^{-1}, and an R928P red-sensitive photomultiplier (range 200–870 nm). An Oxford Instruments Optistat® DN liquid nitrogen bath cryostat was used for the low-temperature measurements. The solutions were freshly prepared prior to the measurements in the following way: the dried ionic liquid was heated to 70 °C; the Eu dimer was dissolved in the ionic liquid and left to stir for 2 h at 50 °C under high vacuum. The solutions had a concentration of approximately 2.5×10^{-3} M. To check the influence of slow kinetics, the same solutions were measured at different times over a period of several weeks. The luminescence spectra did not show any changes during this time period.

NMR spectroscopy: ^{1}H and ^{13}C NMR spectra were recorded on a Bruker Avance 400 MHz NMR spectrometer, and ^{89}Y NMR spectra were recorded on a Bruker Superconducting Fourier transform NMR spectrometer Avance II 600 MHz.

EXAFS: EXAFS measurements were carried out in transmission mode using a Si(111) double crystal monochromator on the Dutch–Belgian Beamline (DUBBLE, BM26 A) at the European Synchrotron Radiation Facility (ESRF, Grenoble, France).[89,90] Higher harmonics were rejected by Si mirrors (suppression factor about 1000). The europium L_{III} edge spectra were collected using Oxford Instruments ionization chambers, filled with 30 % N_2 with He for I_0 at ambient temperature and pressure. Data were collected in equidistant k steps of 0.05 Å^{-1} across a k range of 2.5 to 12.7 (limit due to L_{II} edge). An Fe metal foil (first inflection point at 7112 eV) was used for energy calibration. EXAFS data extraction and data fitting was performed using the program EXAFSPAK.[91] Theoretical phase and amplitude functions were calculated using FEFF 8.2 using the crystal structure of compound **2**.[92] The amplitude reduction factor S_0^2 was kept constant at 1.0 throughout the fit.

HEXS: HEXS experiments were carried out at beamline ID15B of the European Synchrotron Radiation Facility (ESRF, Grenoble, France). A monochromatic beam of energy 87.8 keV was selected using a single (511) bent Laue silicon crystal. The beam size incident on the sample was controlled by a set of tungsten slits just prior to the sample stage. Scattering images in the forward direction were collected on a Pixium 4700 flat panel detector at a sample-detector distance of approximately 300 mm.

Polycarbonate capillaries with a 2 mm diameter were used as sample holders. The scattering signal of the empty capillary was subtracted from each spectrum. The background was corrected with respect to the Compton scattering, and the data normalized using the sum of the form factors, which had been estimated from the molar ratio of the atoms in each sample.

FTIR spectra were recorded on a Bruker IFS-66 spectrometer, with the ionic liquid and metal complexes dispersed between two NaBr windows, or by making a mull with nujol (for the metal complexes). Elemental analyses (CHN) were done on a CE Instruments EA-1110 elemental analyzer.

Acknowledgements

We acknowledge the FWO-Vlaanderen (project G.0508.07) and the KU Leuven (project GOA 08/05 and project IDO/05/005) for financial support. We also thank IoLiTec (Denzlingen, Germany) for support of this research. R.V.D. thanks the FWO-Vlaanderen for a travel grant, which allowed him to spend 6 months at the European Synchrotron Radiation Facility (ESRF, Grenoble, France) between November 1, 2007, and April 30, 2008. We thank the FWO-Vlaanderen and the Netherlands Organization for Scientific Research (NWO) for providing beam time at the Dutch–Belgian Beamline (DUBBLE, BM26A, ESRF). In-house beam time at ID15B (ESRF) was kindly provided by Dr. Veijo Honkimäki, head of the high-energy scattering beamline ID15 at the ESRF. Infrared spectra and CHN analyses were obtained by Dirk Henot. Dr. Wim Bras (DUBBLE) is acknowledged for helpful discussions and support.

[1] T. Welton, *Chem. Rev.* **1999**, *99*, 2071–2083.
[2] P. Wasserscheid, W. Keim, *Angew. Chem.* **2000**, *112*, 3926–3945; *Angew. Chem. Int. Ed.* **2000**, *39*, 3772–3789.
[3] K. R. Seddon, *J. Chem. Technol. Biotechnol.* **1997**, *68*, 351–356.
[4] P. Bonhôte, A. P. Dias, N. Papageorgiou, K. Kalyanasundaram, M. Grätzel, *Inorg. Chem.* **1996**, *35*, 1168–1178.
[5] H. Olivier-Bourbigou, L. Magna, *J. Mol. Catal. A* **2002**, *182*, 419–437.
[6] A. J. Carmichael, M. J. Earle, J. D. Holbrey, P. B. McCormac, K. R. Seddon, *Org. Lett.* **1999**, *1*, 997–1000.
[7] J. Dupont, R. F. de Souza, P. A. Z. Suarez, *Chem. Rev.* **2002**, *102*, 3667–3691.
[8] A. E. Visser, R. P. Swatloski, W. M. Reichert, R. Mayton, S. Sheff, A. Wierzbicki, J. H. Davis, Jr., R. D. Rogers, *Environ. Sci. Technol.* **2002**, *36*, 2523–2529.
[9] A. Ouadi, B. Gadenne, P. Hesemann, J. J. E. Moreau, I. Billard, C. Gaillard, S. Mekki, G. Moutiers, *Chem. Eur. J.* **2006**, *12*, 3074–3081.
[10] S. Mekki, C. M. Wai, I. Billard, G. Moutiers, J. Burt, B. Yoon, J. S. Wang, C. Gaillard, A. Ouadi, P. Hesemann, *Chem. Eur. J.* **2006**, *12*, 1760–1766.
[11] F. Endres, M. Bukowski, R. Hempelmann, H. Natter, *Angew. Chem.* **2003**, *115*, 3550–3552; *Angew. Chem. Int. Ed.* **2003**, *42*, 3428–3430.
[12] A. P. Abbott, G. Capper, B. G. Swain, D. A. Wheeler, *Trans. Inst. Met. Finish.* **2005**, *83*, 51–53.
[13] S. Schaltin, P. Nockemann, B. Thijs, K. Binnemans, J. Fransaer, *Electrochem. Solid-State Lett.* **2007**, *10*, D104–D107.
[14] N. Papageorgiou, Y. Athanassov, M. Armand, P. Bonhôte, H. Pettersson, A. Azam, M. Grätzel, *J. Electrochem. Soc.* **1996**, *143*, 3099–3108.
[15] P. Wang, S. M. Zakeeruddin, J.-E. Moser, M. Grätzel, *J. Phys. Chem. B* **2003**, *107*, 13280–13285.
[16] K. Lunstroot, K. Driesen, P. Nockemann, C. Görller-Walrand, K. Binnemans, S. Bellayer, J. Le Bideau, A. Vioux, *Chem. Mater.* **2006**, *18*, 5711–5715.
[17] A. Taubert, *Acta Chim. Slov.* **2005**, *52*, 183–186.
[18] M. Hasan, I. V. Kozhevnikov, M. Rafiq, H. Siddiqui, C. Femoni, A. Steiner, N. Winterton, *Inorg. Chem.* **2001**, *40*, 795–800.
[19] J. B. Willems, H. W. Rohm, C. Geers, M. Köckerling, *Inorg. Chem.* **2007**, *46*, 6197–6203.
[20] Y. Zhou, M. Antonietti, *Adv. Mater.* **2003**, *15*, 1452–1455.
[21] T. Nakashima, N. Kimizuka, *J. Am. Chem. Soc.* **2003**, *125*, 6386–6387.
[22] A. Taubert, *Angew. Chem.* **2004**, *116*, 5494–5496; *Angew. Chem. Int. Ed.* **2004**, *43*, 5380–5382.
[23] A. Taubert, Z. Li, *Dalton Trans.* **2007**, 723–727.
[24] P. Nockemann, B. Thijs, N. Postelmans, K. Van Hecke, L. Van Meervelt, K. Binnemans, *J. Am. Chem. Soc.* **2006**, *128*, 13658–13659.
[25] Y. Yoshida, J. Fujii, G. Saito, T. Hiramatsu, N. Sato, *J. Mater. Chem.* **2006**, *16*, 724–727.
[26] I. J. B. Lin, C. S. Vasam, *J. Organomet. Chem.* **2005**, *690*, 3498–3512.
[27] M. Hasan, I. V. Kozhevnikov, M. R. H. Siddiqui, A. Steiner, N. Winterton, *Inorg. Chem.* **1999**, *38*, 5637–5641.
[28] K. Binnemans, *Chem. Rev.* **2007**, *107*, 2592–2614.
[29] J.-H. Liao, W.-C. Huang, *Inorg. Chem. Commun.* **2006**, *9*, 1227–1231.
[30] J. H. Liao, P. C. Wu, W. C. Huang, *Cryst. Growth Des.* **2006**, *6*, 1062–1063.
[31] W. M. Reichert, J. D. Holbrey, K. B. Vigour, T. D. Morgan, G. A. Broker, R. D. Rogers, *Chem. Commun.* **2006**, 4767–4779.

[32] J. D. Holbrey, K. B. Vigour, W. M. Reichert, R. D. Rogers, *J. Chem. Crystallogr* **2006**, *36*, 799–804.
[33] K. Jin, X. Huang, L. Pang, J. Li, A. Appel, S. Wherland, *Chem. Commun.* **2002**, 2872–2873.
[34] A. Babai, A. V. Mudring, *Inorg. Chem.* **2006**, *45*, 3249–3255.
[35] A. Babai, A. V. Mudring, *Chem. Mater.* **2005**, *17*, 6230–6238.
[36] P. Nockemann, B. Thijs, K. Van Hecke, L. Van Meervelt, K. Binnemans, *Cryst. Growth Des.* **2008**, *8*, 1353–1363.
[37] C. C. Hines, V. A. Cocalia, R. D. Rogers, *Chem. Commun.* **2008**, 226–228.
[38] C. C. Hines, D. B. Cordes, S. T. Griffin, S. I. Watts, V. A. Cocalia, R. D. Rogers, *New J. Chem.* **2008**, *32*, 872–877.
[39] L. N. Puntus, K. J. Schenk, J.-C. G. Bünzli, *Eur. J. Inorg. Chem.* **2005**, 4739–4744.
[40] E. Guillet, D. Imbert, R. Scopelliti, J.-C. G. Bünzli, *Chem. Mater.* **2004**, *16*, 4063–4070.
[41] P. Nockemann, E. Beurer, K. Driesen, R. Van Deun, K. Van Hecke, L. Van Meervelt, K. Binnemans, *Chem. Commun.* **2005**, 4354–4356.
[42] K. Driesen, P. Nockemann, K. Binnemans, *Chem. Phys. Lett.* **2004**, *395*, 306–310.
[43] S. Arenz, A. Babai, K. Binnemans, K. Driesen, R. Giernoth, A. V. Mudring, P. Nockemann, *Chem. Phys. Lett.* **2005**, *402*, 75–79.
[44] I. Billard, S. Mekki, C. Gaillard, P. Hesemann, G. Moutiers, C. Mariet, A. Labet, J.-C. G. Bünzli, *Eur. J. Inorg. Chem.* **2004**, 1190–1197.
[45] A. Chaumont, G. Wipff, *Chem. Eur. J.* **2004**, *10*, 3919–3930.
[46] A. E. Visser, R. D. Rogers, *J. Solid State Chem.* **2003**, *171*, 109–113.
[47] A. E. Visser, R. P. Swatloski, S. T. Griffin, D. H. Hartman, R. D. Rogers, *Sep. Sci. Technol.* **2001**, *36*, 785–804.
[48] P. Nockemann, B. Thijs, S. Pittois, J. Thoen, C. Glorieux, K. Van Hecke, L. Van Meervelt, B. Kirchner, K. Binnemans, *J. Phys. Chem. B* **2006**, *110*, 20978–20992.
[49] C. Gaillard, I. Billard, A. Chaumont, S. Mekki, A. Ouadi, M. A. Denecke, G. Moutiers, G. Wipff, *Inorg. Chem.* **2005**, *44*, 8355–8367.
[50] C. Hardacre, J. D. Holbrey, M. Nieuwenhuyzen, T. G. A. Youngs, *Acc. Chem. Res.* **2007**, *40*, 1146–1155.
[51] C. Bessada, A. Rakhmatullin, A.-L. Rollet, D. Zanghi, *J. Nucl. Mater.* **2007**, *360*, 43–48.
[52] S. Samikkanu, K. Mellem, M. Berry, P. S. May, *Inorg. Chem.* **2007**, *46*, 7121–7128.
[53] J.-C. G. Bünzli, G. R. Choppin in *Lanthanide Probes in Life, Chemical and Earth Sciences—Theory and Practice*, Elsevier, Amsterdam, **1989**.
[54] C. Görller-Walrand, K. Binnemans in *Handbook on the Physics and Chemistry of Rare Earths Vol. 25* (Eds: K. A. Gschneidner, Jr., L. Eyring), North-Holland, Amsterdam, **1998**, Chapter 167, pp. 101–264.
[55] S. W. Magennis, S. Parsons, A. Corval, J. D. Woollins, Z. Pikramenou, *Chem. Commun.* **1999**, 61–62.
[56] S. W. Magennis, S. Parsons, Z. Pikramenou, *Chem. Eur. J.* **2002**, *8*, 5761–5771.
[57] P. B. Glover, A. P. Bassett, P. Nockemann, B. M. Kariuki, R. Van Deun, Z. Pikramenou, *Chem. Eur. J.* **2007**, *13*, 6308–6320.
[58] K. Binnemans, C. Görller-Walrand, *J. Rare Earths* **1996**, *14*, 173–180.
[59] B.-K. Teo, *EXAFS: basic principles and data analysis*, Springer-Verlag, Berlin, **1986**.
[60] D. C. Koeningsberger, R. Prins, *X-ray Absorption: principles, applications and techniques of EXAFS, SEXAFS and XANES*, Wiley, New York, **1988**.
[61] J. E. Penner-Hahn, *Coord. Chem. Rev.* **1999**, *190–192*, 1101–1123.
[62] D. T. Bowron, G. A. Saunders, R. J. Newport, B. D. Rainford, H. B. Senin, *Phys. Rev. B* **1996**, *53*, 5268–5275.
[63] Y. Tao, G. W. Zhao, X. Ju, X. G. Shao, W. P. Zhang, S. D. Xia, *Mater. Lett.* **1996**, *28*, 137–140.
[64] P. M. Peters, S. N. Houde Walter, *Appl. Phys. Lett.* **1997**, *70*, 541–543.
[65] F. D′Acapito, S. Mobilio, L. Santos, R. M. Almeida, *Appl. Phys. Lett.* **2001**, *78*, 2676–2678.
[66] G. Mountjoy, J. M. Cole, T. Brennan, R. J. Newport, G. A. Saunders, G. W. Wallidge, *J. Non-Cryst. Solids* **2001**, *279*, 20–27.
[67] J. Naslund, P. Lindqvist-Reis, I. Persson, M. Sandstrom, *Inorg. Chem.* **2000**, *39*, 4006–4011.
[68] K. Servaes, C. Hennig, R. Van Deun, C. Görller-Walrand, *Inorg. Chem.* **2005**, *44*, 7705–7707.
[69] M. Harada, T. Okada, *J. Solution Chem.* **2006**, *35*, 1645–1654.
[70] K. Servaes, C. Hennig, I. Billard, C. Gaillard, K. Binnemans, C. Görller-Walrand, R. Van Deun, *Eur. J. Inorg. Chem.* **2007**, 5120–5126.
[71] M. A. Denecke, *Coord. Chem. Rev.* **2006**, *250*, 730–754.
[72] C. Hennig, K. Servaes, P. Nockemann, K. Van Hecke, L. Van Meervelt, J. Wouters, L. Fluyt, C. Görller-Walrand, R. Van Deun, *Inorg. Chem.* **2008**, *47*, 2987–2993.
[73] A. E. Visser, M. P. Jensen, I. Laszak, K. L. Nash, G. R. Choppin, R. D. Rogers, *Inorg. Chem.* **2003**, *42*, 2197–2199.
[74] M. P. Jensen, J. Neuefeind, J. V. Beitz, S. Skanthakumar, L. Soderholm, *J. Am. Chem. Soc.* **2003**, *125*, 15466–15473.
[75] V. A. Cocalia, M. P. Jensen, J. D. Holbrey, S. K. Spear, D. C. Stepinski, R. D. Rogers, *Dalton Trans.* **2005**, 1966–1971.
[76] A. Chaumont, G. Wipff, *Phys. Chem. Chem. Phys.* **2006**, *8*, 494–502.
[77] V. A. Cocalia, K. E. Gutowski, R. D. Rogers, *Coord. Chem. Rev.* **2006**, *250*, 755–764.
[78] S. I. Nikitenko, C. Hennig, M. S. Grigoriev, C. Le Naour, C. Cannes, D. Trubert, E. Bossé, C. Berthon, P. Moisy, *Polyhedron* **2007**, *26*, 3136–3142.
[79] C. Hardacre, *Annu. Rev. Mater. Res.* **2005**, *35*, 29–49.
[80] J. Neuefeind, S. Skanthakumar, L. Soderholm, *Inorg. Chem.* **2004**, *43*, 2422–2426.
[81] L. Soderholm, J. Neuefeind, S. Skanthakumar, *Anal. Bioanal. Chem.* **2005**, *383*, 48–55.
[82] S. Skanthakumar, L. Soderholm, *Mater. Res. Soc. Symp. Proc.* **2006**, *893*, 411–416.
[83] C. Hennig, A. Ikeda, K. Schmeide, V. Brendler, H. Moll, S. Tsushima, A. C. Scheinost, S. Skanthakumar, R. Wilson, L. Soderholm, K. Servaes, C. Görller-Walrand, R. Van Deun, *Radiochim. Acta* **2008**, *96*, 607–611.
[84] G. Stein, E. Würzberg, *J. Chem. Phys.* **1975**, *62*, 208–213.
[85] P. S. Coan, L. G. Hubert-Pfalzgraf, K. G. Caulton, *Inorg. Chem.* **1992**, *31*, 1262–1267.
[86] P. Nockemann, K. Binnemans, K. Driesen, *Chem. Phys. Lett.* **2005**, *415*, 131–136.
[87] SAINT, Bruker Analytical X-ray Systems Inc., Madison, WI, Manual Version 5/6.0, **1997**.
[88] SHELXTL-PC, Bruker Analytical X-ray Systems Inc., Madison, WI, Manual Version 5.1, **1997**.
[89] M. Borsboom, W. Bras, I. Cerjak, D. Detollenaere, D. G. van Loon, P. Goedtkindt, M. Konijnenburg, P. Lassing, Y. K. Levine, B. Munneke, M. Oversluizen, R. van Tol, E. Vlieg, *J. Synchrotron Radiat.* **1998**, *5*, 518–520.
[90] S. Nikitenko, A. M. Beale, A. van der Eerden, S. D. M. Jacques, O. Leynaud, D. Detollenaere, R. Kaptein, B. M. Weckhuysen, W. Bras, *J. Synchrotron Radiat.* **2008**, *15*, 632–640.
[91] G. N. George, I. J. Pickering, *EXAFSPAK, a suite of computer programs for analysis of X-ray absorption spectra*, Stanford Synchrotron Radiation Laboratory, Stanford, **2000**.
[92] A. L. Ankudinov, B. Ravel, J. J. Rehr, S. D. Conradson, *Phys. Rev. B* **1998**, *58*, 7565–7576.

Received: July 13, 2008
Published online: January 2, 2009

